An Inelastic Neutron Scattering Vibrational Spectroscopy Study of Hydrated Melanin

J. A. Martinez-Gonzalez[a†], H. Cavaye[a], J.D. Mcgettrick[b], P. Meredith[c], K. A. Motovilov[d], A. B. Mostert[e*]

[a] ISIS Neutron and Muon Source, Rutherford Appleton Laboratory, Science and Technology Facilities Council, Didcot, OX11 0QX, UK

[b] SPECIFIC, Swansea University, College of Engineering, Bay Campus, Fabian Way, Crymlyn Burrows, Swansea, SA1 8EN, UK

[c] Department of Physics, Swansea University, Singleton Park, SA2 8PP, Wales, UK

[d] Moscow Institute of Physics and Technology, 141701, Institutsky lane 9, Dolgoprudny, Russia

[e] Department of Chemistry, Swansea University, Singleton Park, SA2 8PP, Wales, UK

*Corresponding Author: a.b.mostert@swansea.ac.uk

†Current Address: Donostia International Physics Center, Paseo Manuel de Lardizabal 4, 20018, San Sebastian, Spain.

Abstract

The importance of electrically functional biomaterials is increasing as researchers explore ways to utilise them in novel sensing capacities. It has been recognised that for many of these materials the state of hydration is a key parameter that can heavily affect the conductivity, particularly those that rely upon ionic or proton transport as a key mechanism. However, thus far little attention has been paid to the nature of the water morphology in the hydrated state and the concomitant ionic conductivity. Presented here is an inelastic neutron scattering (INS) experiment on hydrated eumelanin, a model bioelectronic material, in order to investigate its 'water morphology'. We develop a rigorous new methodology for performing hydration dependent INS experiments. We also model the eumelanin dry spectra with a minimalist approach whereas for higher hydration levels we are able to obtain difference spectra to extract out the water scattering signal. A key result is that the physi-sorbed water structure within eumelanin is dominated by interfacial water with the number of water layers between 3-5, and no bulk water. We also detect for the first time, the potential signatures for proton cations, most likely the Zundel ion, within a biopolymer/water system. These new signatures may be general for soft proton ionomer systems, if the systems are comprised of only interfacial water within their structure. The nature of the water morphology opens up new questions about the potential ionic charge transport mechanisms within hydrated bioelectronics materials.

Key Words: Melanin, Bioelectronics, Inelastic Neutron Scattering, Hydration Control, Vibrational structure, Zundel cation.

Introduction

Bioelectronics is a rapidly emerging field at the intersection of the physical, chemical and life sciences.[1-9] One of the aims of the field is to address some of the major challenges of the 21st century as outlined for example by the US National Academy of Engineering, which has presented the need of "advance health informatics" among its 14 grand challenges for engineering in the 21st century.[10] As such, there is a constant search to create new devices for medical interventions, biosensors, monitoring devices etc. that can directly read or write biological signals with conventional semiconductor-based electronics.[1-9]

It is becoming apparent that a key parameter to control the conductivity of bioelectronic materials and devices is the water content of the system, since the degree of hydration can impact the behaviour of materials and the performance of devices, especially proton conductivity.[11] Hence, natural questions arise: what is the structure of water in these materials, and how does it influence charge transport?

Given the extensive range of prominent materials explored within the community including PEDOT:PSS[12-14], chitosan[15, 16], melanin[17-19], reflectin[20, 21], glycosaminoglycans[22, 23], polyaniline[24], serum-albumin[25], polyethylene oxide[26], nafion[27, 28], and poly(ethylenimine)[29], only recently have serious questions being asked about water structure as a function of hydration – an example being serum-albumin[30]. In this study electrical measurements were used to infer the local water structure and concomitant proton transport as the material was systematically hydrated. However, electrical measurements by their nature cannot probe the actual water morphology. As such, a new approach is needed. Presented herein is an inelastic neutron scattering (INS) experiment performed on the bioelectronic material eumelanin as a function of hydration. This study is envisaged as a starting point for probing the internal water structure of a hydrated bioelectronic material and connecting said structure to the proton conduction mechanism.

Eumelanin, or in common parlance just melanin,[31] has been selected for this work since it is proving to be a model bioelectronic material[11] that acts as an interfacial ionomer for various device applications.[32-36] Coupled with its hygroscopic nature[37, 38] and the clear modulation of its proton conductivity as a function of hydration,[17-19, 34, 39] and electronic redox properties [36, 40] it is a promising potential candidate to begin to answer the questions of water structure and concomitant proton transport questions in bioelectronic materials.

The INS technique is used to probe the vibrational spectra of amorphous and crystalline materials.[41, 42] As the name suggests, when a neutron with appropriate kinetic energy is scattered inelastically from a sample, the energy that is transferred will excite vibrational modes within the sample. By monitoring the energy loss of the scattered neutrons, a vibrational spectrum analogous to those obtained by optical methods (e.g., infra-red absorption or Raman spectroscopy) can be produced from which the vibrational structure of the material can be inferred. An INS spectrum is highly complementary to such optically-obtained spectra, having a number of benefits for hydrogen-containing materials in particular.[43] Firstly, there are no optical selection rules with INS; all modes are active and a single INS spectrum may show all the modes of interest. Secondly, the intensity of modes in an INS spectrum is directly related to the concentration, neutron scattering power and displacement vectors of the nuclei involved. Therefore, compared to infrared (IR) spectroscopy and Raman scattering, INS spectra are relatively easy to predict. Lastly, the highly penetrating nature of neutrons means that INS is ideal for studying the bulk properties of a sample, without needing to worry about surface effects or sampling bias.

Hydrogen in particular has a very large (incoherent) neutron scattering cross-section, which means that INS is uniquely suited to studying the vibrational properties of the protons in melanin and hydrated melanin. In this study we use INS to investigate the vibrational structure of melanin and how this changes upon hydration. The penetrating nature of the neutrons allowed the samples to be fully sealed, aiding the rigorous hydration procedure. We then simulate the spectra of a number of simple molecular building blocks in order to gain insight into the complex and poorly characterised structure of melanin itself.

Overall, the work presented here is a significant advance on the use of the INS technique as it pertains to hygroscopic materials by utilising a new method of hydrating materials. We do this to probe the structure of water in the bioelectronic material melanin and the potential consequences for proton charge transport.

Experimental Methods & Baseline Chemical and Physiochemical Analysis

Material Synthesis: Melanin was synthesized following a standard literature procedure.[37, 44, 45] In brief, D,L-dopa (Sigma-Aldrich) was dissolved in deionized water, subsequently adjusted to and maintained at pH 8 using NH_3 (28%) as air was bubbled through the solution while being stirred for 3 days. Keeping the maximum pH at 8 ensured that ring fission of the indolequinone moieties are kept to a minimum ensuring a biomimetic material.[45] Afterwards, the solution was brought to pH 2 using aqueous HCl (32%) to precipitate the pigment. The solution was then filtered and washed multiple

times with deionized water and dried. Four batches were synthesized and then homogenized to obtain the material for the study.

Melanin Characterization: The samples were confirmed as melanin via UV-Vis absorbance spectroscopy, electron paramagnetic resonance (EPR) and x-ray photoelectron spectroscopy (XPS).

For the UV-Vis absorbance spectroscopy a small amount of melanin powder was dissolved in a pH 8 deionised water solution (adjusted with NH_3). Spectra were then obtained utilising a Perkin Elmer PDA UV/Vis Lambda 265, utilising the wavelength monitoring functionality, obtaining a wavelength range from 350 nm to 900 nm at 1nm wavelength intervals. Example data can be seen in Figure 1A, where the featureless, exponential spectra as a function of wavelength is as expected for melanin[46].

For the EPR measurement, a powder sample of the melanin was measured using a Bruker EMX Micro X, CW-EPR spectrometer with an E4104 X-band cavity at a microwave power of 0.87 mW at room temperature. The spectra was taken at a modulation frequency of 100 kHz, modulation amplitude of 1 Gauss with a scan width of 60 Gauss. The apparent isotropic g factor was calibrated against a DPPH standard and found to be 2.0036, which is as reported elsewhere for solid melanin synthesized in the same manner[47-49]. An example spectrum can be seen in Figure 1B.

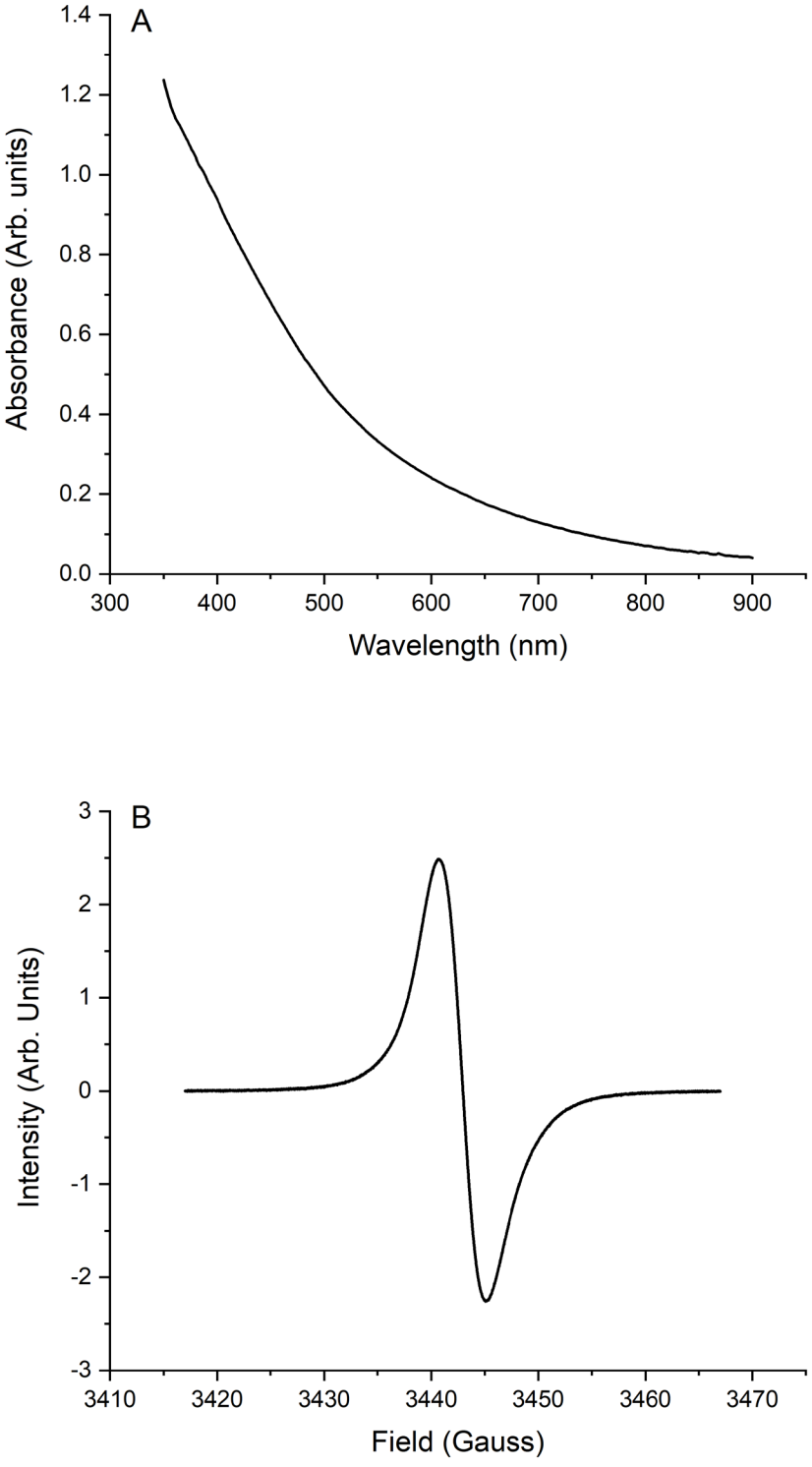

Figure 1. A) An example UV-Vis absorbance spectrum obtained for the melanin sample. The curve shows a simple decaying exponential as expected for the material. B) An example CW-EPR X-band spectrum obtained for the sample and is as expected from extensive literature.

For the XPS elemental analysis, data was obtained via a XPS wide-scan survey spectrum of pressed pellets of the powder utilizing a Kratos Axis Supra with a 225 W AlKα X-ray source with an emission current of 15 mA and equipped with a quartz crystal monochromator with a 500 mm Rowland circle. Higher resolution spectra were then collected in triplicate for quantification with a pass energy of 40 eV, with the hybrid lens setting, 0.1 eV step size, 1 s dwell time for electron counting at each step. The integral Kratos charge neutralizer was used as an electron source to eliminate differential charging. The atomic compositions thus obtained can be seen in Table 1 and are compatible with that of a synthetic melanin. We note that elemental surface scans of melanins are representative of the bulk as previously demonstrated[50].

Table 1. The atomic composition (atomic concentration %) and atomic ratios determined from pressed powder pellets of the synthetic melanin sample. For comparison the expected ratios for the monomer building blocks DHI and DHICA are shown where it is expected that a melanin sample's values will fall roughly in-between the two monomer building block's values.

Sample	C (at%)	O (at%)	N (at%)	C/N	O/N	C/O
DHI - Expected	72.7	18.2	9.1	8	2	4
DHICA - expected	64.3	29.6	7.1	9	4	2.2
Sample	69.5±0.3	21.2±0.4	9.2±0.2	7.6	2.3	3.3

Finally, to quantify the water content of the powder melanin as a function of relative pressure/relative humidity, an adsorption isotherm was obtained. The method for obtaining a water adsorption curve was as previously published[37, 51]. In brief, a vacuum capable microbalance (CI Electronics Ltd.) was attached to a vapour delivery system in which vapour was introduced from a flask containing H_2O (de-ionised, freeze-pump-thaw 3 times). Pressure measurements were obtained using a calibrated BOC-Edwards GK series 0−50 mbar gauge, and a dry scroll pump was used to create the vacuum. For adsorption measurements as a function of relative pressure (note 100 times relative pressure is the relative humidity), the desired pressure of H_2O was admitted into the system, and the reservoir was closed off. The sample was allowed to equilibrate for a couple of hours while the sample mass was monitored with the microbalance. For the next data point, the pressure was increased again and allowed to come to equilibrium. The procedure was then repeated. The experiments were conducted at a constant temperature of 22.2 ± 0.9 °C. Uncertainties in the results were calculated by convoluting the random errors in the estimated dry weight of the powder with that of the final weight and then propagated. The data obtained can be seen in Figure 2. The data was fitted to a limited layers Brunauer-Emmett-Teller (BET) model to the a range of 0.05 to 0.35 as is standard[52]:

$$\frac{n^{\sigma}}{n_m^{\sigma}} = \frac{ZX}{1-X}\frac{1-(\nu+1)X^{\nu}+\nu X^{\nu+1}}{(Z-1)X-ZX^{\nu+1}}$$

where $n^{\sigma}$is the number of moles of adsorbate, n_m^{σ} is the number of moles required to give monolayer coverage, X is the relative pressure of the adsorbate, ν is the number of monolayers and $Z = e^{E_d - E_a/RT}$. Parameters E_d and E_a are enthalpy of desorption and adsorption respectively, R is the universal gas constant and T is temperature. The BET parameters are summarised in Table 2. Note that the water adsorbed is slightly more than previously reported[37, 51], but the adsorption parameters are otherwise similar to what one would expect. Previous reports were on pressed powder pellets of melanin whereas Figure 2 is for a powder, hence a greater surface area is available for adsorption.

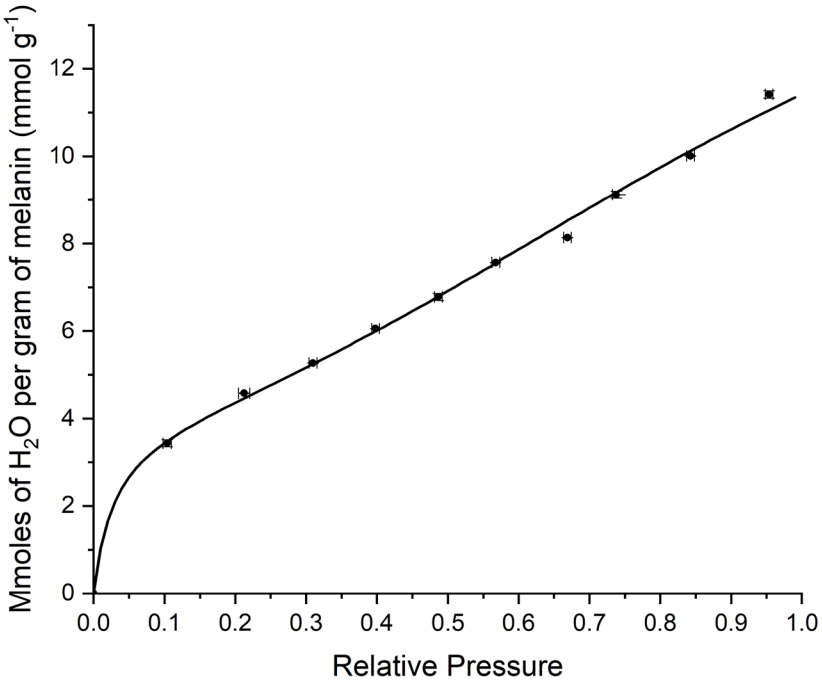

Figure 2. The adsorption isotherm data obtained on powdered melanin sample points with error bars). Also shown is the limited layers BET model (solid line).

Table 2. The BET modelling parameters obtained for the adsorption isotherm data depicted in Figure 2. Parameters for pressed powder pellets of melanin are also included for comparison.

Morphology	$E_d - E_a$ (kJ mol^{-1})	n_m^{σ} (mmol g^{-1})	ν (no.)
Powder (this work)	8.7±1.1	3.9±2.6	4.9
Pellet [37, 51]	7.7	4.7	3.65

Melanin Hydration Procedures for Inelastic Neutron Scattering: The melanin powders were prepared at various hydration levels before being placed within the INS samples holders before loading within the spectrometer. This was achieved by placing the powder in a custom made PTFE holder within a vacuum capable bespoke stainless steel chamber, which had a valve attached to it that enables the chamber to be disconnected from the vacuum line while maintaining the vacuum line atmosphere inside. The chamber was connected via KF16 bellows to a water vial (deionised water, degassed via several freeze-pump-thaw cycles), an Edwards GK series (0 – 50 mbar) pressure gauge, Pirani Gauge (for monitoring the vacuum level) and a dry scroll pump. To dry the melanin, the samples were initially placed within a vacuum oven at 50 °C for at least 24 hours. Just before loading, the sample was then removed and transferred to the aforementioned PTFE holder, which was then immediately placed within the custom made chamber and a vacuum applied. Initially the sample within the chamber was pumped on for several hours to dry at a vacuum level of 10^{-2} mbar. For the dry sample experiment ~ 16 hours was used and as for the other, hydrated samples the initial drying time was ~ 6 – 8 hours.

For the dry sample of melanin, once the 10 hours was reached, the sample stainless steel chamber was isolated and disconnected from the line. The chamber, which was still under vacuum, was transferred into an Argon glove box with a dry atmosphere. The sample chamber was then opened within the glovebox, the sample removed and transferred to an aluminium pouch, which in turn was enclosed within a standard aluminium can holder for the INS experiment on TOSCA (see below). Given the enclosed nature of the aluminium holder, the local dry atmosphere was preserved ensuring that the sample was dry before being loaded into the spectrometer.

The hydrated samples were treated similarly as for the dry, but with some variations to account for water content. After the initial drying period within the hydration chamber, the vacuum pump was first isolated, and then the water vial opened to let in a H_2O atmosphere. Once the desired pressure had been reached, the water vial was isolated, and the sample allowed to come to equilibrium over several hours (4 – 5 hours) at the desired target pressure. The amount of time for ensuring for equilibrium was well beyond the known time required for samples to come to equilibrium as per previously published adsorption isotherms and our experience in obtaining the powder adsorption isotherm (~1 – 2 hours) [37]. During the equilibrium time, both the lab temperature and the pressure was monitored regularly to ensure stability. Final pressures were 0.0 mbar, 3.0 mbar, 15.1 mbar, 20.1 mbar, 24.6 mbar with a measured water saturation vapour pressure of 27.2 mbar, which yielded relative pressures (relative humidities) of 0.0, 0.11 (11%), 0.56 (56%), 0.74 (74%) and 0.90 (90%). Once sufficient time passed, the hydration chamber was isolated and disconnected from the line. The chamber was then transferred into a separate, mobile glovebox within which a hydrated atmosphere was pre-prepared. This

atmosphere was achieved with the use of a large open tray within the box with a saturated salt solutions, where the salt selected was commensurate with the hydration level within the hydration chamber. The amount of time given for the tray to come to equilibrium with the box atmosphere was > 6 hours before sample transfer. Once inside, the melanin sample was removed and placed within a sample holder as per the dry sample. The saturated salts, and their respective relative humidities chosen for the hydrated samples were LiCl (RH = 11%), NaI (RH = 53%) and NaCl (RH = 75%), where the NaCl was also used for the 0.90 relative pressure sample transfer (which we note was rapid). All salts were obtained from Sigma-Aldrich and used as is.

Inelastic Neutron Scattering:

INS spectra[53] were recorded on the indirect geometry spectrometer TOSCA[54, 55] at the ISIS Neutron and Muon Source (Chilton, Oxfordshire, UK).[56] The resolution is ~1.25% of the energy transfer, affording sufficient resolution in the energy range of interest, 0 – 2000 cm^{-1}. Measurements were performed <20 K using a closed cycle refrigerator. Time of flight data were reduced using the Mantid software package[57]. All spectra recorded had the signal from the aluminium sample holder subtracted out, and then normalised to the adsorption isotherm. We note that the adsorption isotherm normalisation was to Figure S1, which is the adsorption isotherm of Figure 2 transformed into total percentage change of hydrogen content relative to the dry sample. The underlying reason is that the signal strength of INS is related to the hydrogen content of the sample. We do not expect a major contribution from other elements since hydrogen has an incoherent scattering length 2 orders of magnitude larger than that for nitrogen, carbon, and oxygen[58].

Computational Modelling:

Inelastic neutron scattering data and computational work has been previously performed on indoles,[59] but not on hydroxyindoles that form the basis of melanin. The basic monomeric structures of melanin evaluated through *Ab initio* calculation are shown in Figure 3. All *Ab initio* calculations of the vibrational transition energies were carried out using Gaussian16[60]. Firstly, the ground-state geometries for each monomer were calculated, followed by the vibrational frequencies, using the DFT approach with Becke's LYP (B3LYP)[61, 62] exchange-correlation functional and the 6-311+G(d,p) basis set for all atoms. The Gaussian16 output data, that includes the vibrational energies and the atomic displacement of the atoms in each mode, was then used to simulate the INS spectra for each monomer using the AbINS[63] function included in the Mantid software package.[57]

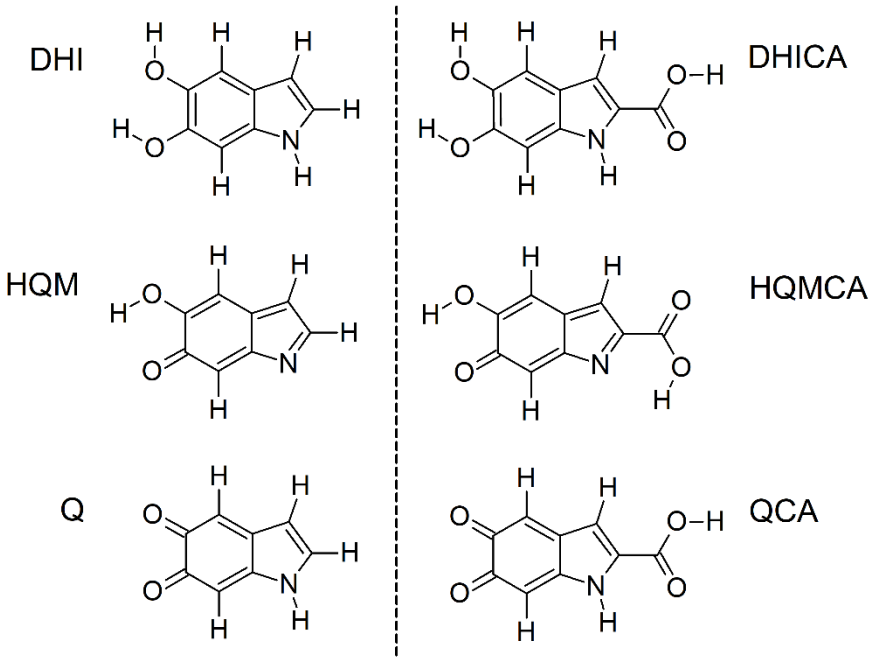

Figure 3. The starting monomer units of melanin (dihydroxyindole – DHI; dihydroxyindole carboxylic acid - DHICA) before the free radical polymerisation step that leads to melanin formation.[64] Also indicated are the various redox states of the starting monomers, which are the hydroquinone methide forms (HQM & HQMCA) and quinone forms (Q & QCA).[31]

Once all the theoretical INS monomer spectra were obtained, we proceeded to construct a linear combination of them, with the aim of replicating the experimentally measured spectrum of melanin itself. The linear combination consisted of 75% quinone, 20% quinone methide, 5% cathechol, which is based upon thermodynamic modelling of a monomer solution at low pH[65], i.e. protonated state as would be expected in the dry sample. Of these 15% of the monomers were assigned a COOH moiety, consistent with the XPS analysis that indicates 15% DHICA/85% DHI if one assumes a monomer system. The main features of the spectra can be identified and characterised, leading to insight into its structure.

Results and Discussion

Presented in Figure 4 are the INS spectra below 2000 cm^{-1} obtained on variously hydrated melanin. As can be seen, there is a clear change in the spectral features as water is added, indicating that more water is present within the sample [compare spectra against an example spectrum for ice-Ih (hexagonal ice, the most common form of ice)]. The most prominent change in features can be seen for the energies ~350 cm^{-1} – 800 cm^{-1}, which indicates the rise of the librational water modes[66, 67]. However, as can be inferred from the spectra of ice-Ih, the features are not as sharp, indicating a lack of crystal structure and hence the formation of “amorphous ice”[68, 69]. This important observation we will return to

later. First, we will discuss the dry spectra of melanin and associated modelling to tease out the underlying features. Once a better understanding of the dry spectra has been obtained, we will then turn to the wet spectra of melanin, and the associated behaviour of the water.

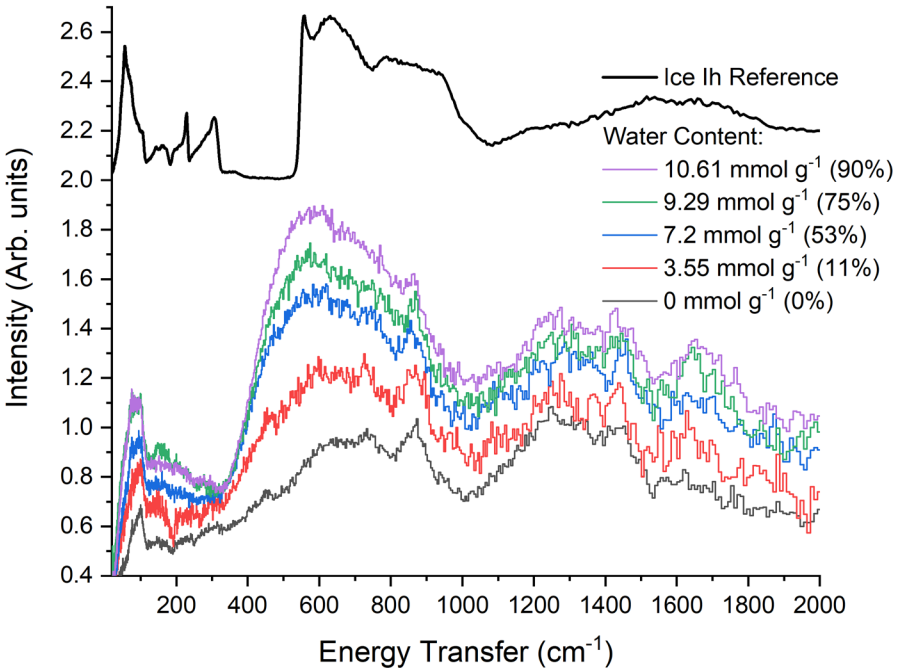

Figure 4. The INS spectra of variously hydrated melanins, normalised to the isotherm in Figure S1. Indicated in the legend are the water contents of the melanins as determined by a water adsorption isotherm on powder melanin (Figure 2) and the corresponding relative humidities. Also shown is the spectrum for ice-Ih as a comparison.

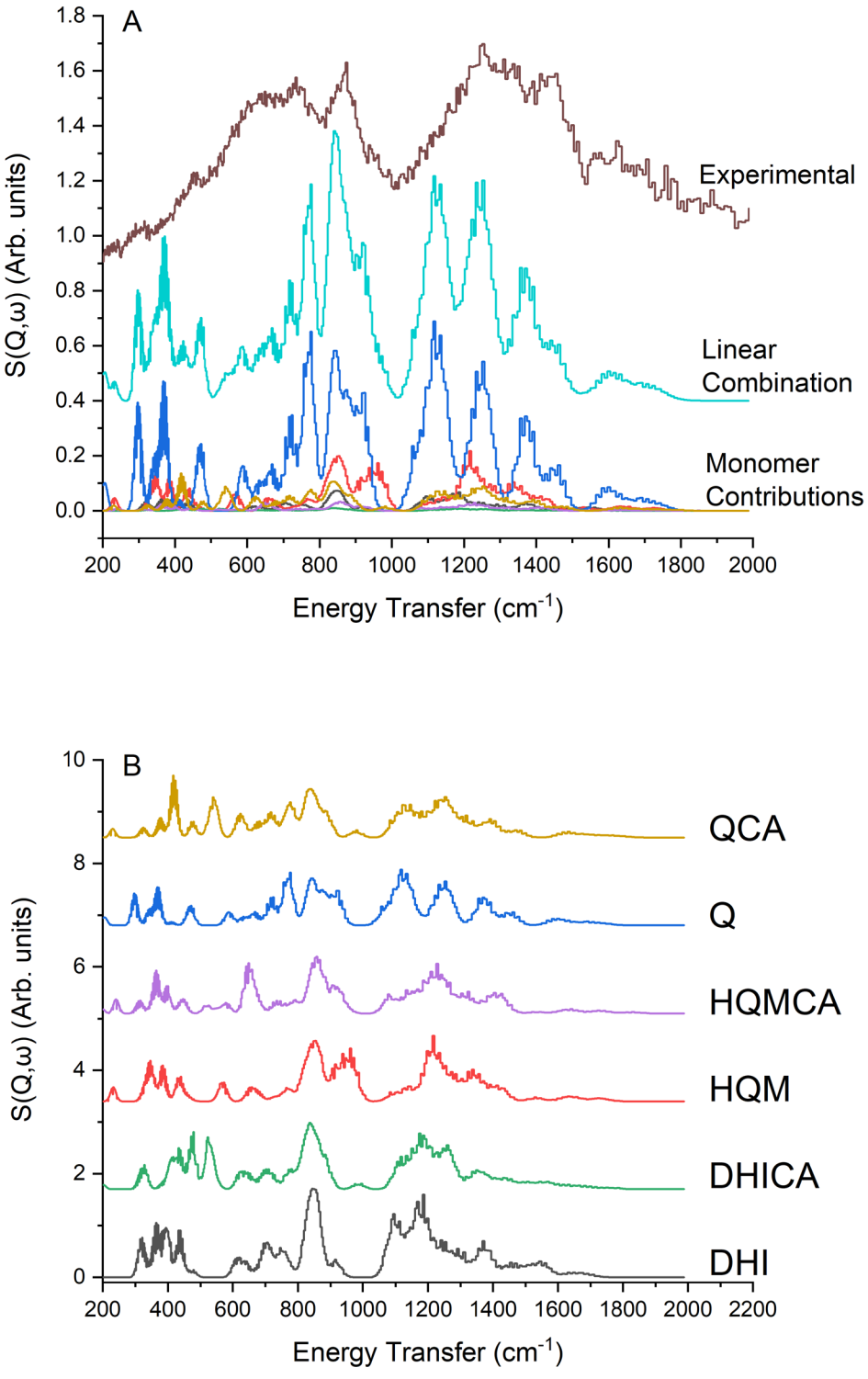

Figure 5. A) The dry melanin INS spectra shown at the top with the modelled linear combination spectrum offset below. At the bottom, the individual monomer contributions are indicated. The individual monomer spectra are shown explicitly in B). The ratios of the monomers were 75% quinone, 20% quinone methide, 5% catechol (based upon thermodynamic modelling of a monomer solution at low pH[65]) with 15% of the monomers having an acid group (see text). B) The labelling of the spectra follows Figure 3.

Turning to the dry data as depicted in Figure 5A. A natural question to ask is whether the dry powder of melanin spectra show any significant contribution from trapped water (i.e. not physi-sorbed water), since it is known that melanin does have bound water within its structure which cannot be removed except via decomposition of the biopolymer[70]. Due to hydrogen having an incoherent scattering length 2 orders of magnitude larger than that for nitrogen, carbon, and oxygen,[58] we can attribute essentially all of the spectral intensity to protons in the samples. When comparing dry spectra to the water signal (below in Figure 6) and ice-Ih, the expected signals/contributions from water, the liberation peaks are essentially absent. One may argue the slight peak in the data 470 cm^{-1} may be a libration peak but could just as well be a melanin signal if one inspects the deconstructed monomer modelled signal below it (which we will explain in due course). As such, trapped water, even though present in dry melanin, does not contribute a significant signal to the dry melanin spectra.

We now turn to understand the INS spectrum of dry melanin in a deeper way. Using a combination of computational and analytical techniques, we developed a simple model in which, by knowing the concentrations of the different monomeric units that form our sample, we could obtain the vibrational modes assignment for the experimental spectrum using the theoretical simulated spectrum as reference.

We note that to date it has not been possible to fully model a melanin stacked particle due to the computationally intensive nature that such a study would entail. The fundamental reason for this state of affairs is that melanin is a chemically heterogeneous compound, derived from the highly reactive monomers that undergo an uncontrolled free radical polymerisation to form various oligomers that subsequently stack in random order. To illustrate this point, a recent article explored 3000 different proto oligomeric structures using DFT and molecular dynamics, but still did not obtain data on stacked systems[71].

Considering these factors, we have taken a simple, minimalist approach to model the INS spectra by obtaining the theoretical INS spectrum for each, small monomeric moiety in isolation. Figure 3 shows the six main monomeric moieties that we expect to be present within the melanin polymer[65]. The resultant spectra for these molecules can be seen in Figure 5B. In general, all monomers have a vibrational gap around 1000 cm^{-1} and another at 1500cm^{-1}. The DHICA has the first gap shifted up to 1100 cm^{-1}. These features mean that the INS spectrum of monomers can be divided into three zones, a first between 200 and 1000 cm^{-1}, the next between 1000 and 1500 cm^{-1} and a last one for vibrations greater than 1500cm^{-1}. Each of the different monomers has a series of characteristic vibrational modes which are considered in the experimental spectrum. If we look at each monomer, we see how the shape of the QCA has a high intensity peak and 3 peaks with medium intensity, the Q monomer one has 4

peaks with great and one with medium intensity. The HQMCA and HQM monomers shape have 3 peaks with high and 2 and 3 peaks with medium intensity respectively. Finally, HQMCA and HQM monomers shape have 3 and 2 peaks with great intensity only.

Next step is modelling the INS spectrum of melanin itself. We combine each individual theoretical INS spectrum via a linear combination trying to obtain the experimental spectrum for the full melanin sample (Figure 5A). The contribution of each monomer spectrum to the linear combination was determined from thermodynamic modelling elsewhere, based upon solutions at low pH[65] (i.e. fully protonated species as expected in the dry solid state). Our approach affords a simulated melanin INS spectrum (Figure 5A, light blue line). Given that a more heterogeneous chemical environment, the broadening of the simulated spectra can well be anticipated, which makes the simulation reasonably good in agreement with the experiment (Figure 5A, brown line), allowing us to use this simple computational approach that avoids an unfeasible full melanin polymer chain computational calculation.

Now that we have the INS melanin simulated spectrum, we can interrogate the vibrational modes in the simulated spectra allowing us to broadly assign the peaks in the experimental spectrum. Starting at the higher energy, the features around 1600-1800 cm^{-1} can be attributed to C=O stretches, particularly in the Q monomers, as well as C=C stretches within the aromatic ring. Ordinarily, due to the low neutron scattering cross-sections of C and O nuclei, these modes would not be visible in an INS spectrum. However, the fused ring structure of the monomers leads to associated displacement of H atoms, which in turn provide INS intensity that we are seeing here. The feature between 1400-1500 cm^{-1} can be attributed to in-plane N-H, O-H, and C-H bending as well as further C-C stretches within the 5-membered ring structures. The broad feature from 1100-1400 cm^{-1} clearly comprises a number of different vibrations, including more C-C stretches in the ring system (primarily antisymmetric in nature), which leads to in plane wagging of the terminal H atoms. Moving down to the prominent feature centred at 900 cm^{-1} we can see both symmetric and asymmetric out of plane C-H bending modes and breathing modes of both the 5-membered ring and the complete indole moiety.

Continuing to the feature around 750-800 cm^{-1} we can identify additional out of plane C-H bending modes and in plane and out of plane ring deformations. The remaining broad feature between 500-750 cm^{-1} includes out of plane O-H bends (especially from the acid-containing monomers such as QCA), as well as symmetric out of plane C-H bends. It is worth noting at this point that this last part of the theoretical spectrum matches the experimental spectrum less well than in the higher energy regions. We believe that the difference is due to our simple approach that does not include the intermonomer

and intermolecular interactions that could be expected in a bulk solid sample of a full melanin polymer. These low-energy and longer-range vibrational modes would require a larger number of computational calculations (for dimers, trimers, tetramers, etc.) and sophisticated analytical tools to combine the INS simulated spectra. This implies more computational cost and it is not clear whether it will ensure a better description than that presented in this work already. All of the above features are summarised in Table 3.

Table 3. Summary of the major features for the INS spectra for dry melanin at <30 K as simulated and depicted in Figure 5A.

Energy (cm^{-1})	Putative Vibrational Mode
500-750	O-H Bend, out of plane
	symmetric C-H Bend, out of plane
750-800	additional C-H Bend, out of plane
	Ring Deformation (in/out plane)
800-900	symmetric & asymmetric C-H Bend, out of plane
	5-membered ring Breathing
1100-1400	antisymmetric C-C, 5-membered ring
1400-1500	N-H Bend, in plane
	O-H Bend, in plane
	C-H Bend, in plane
	C-C stretches, 5-membered ring
1600-1800	C=O stretch
	C-C stretch, aromatic ring

Having interrogated the dry spectra, we turn to the hydration dependent features of the INS spectra. By subtracting the dry spectra, discussed in Figure 5A, from the INS spectra presented in Figure 4, one obtains a difference spectra that represents the water component alone (Figure 6). For aid, the spectra for ice-Ih is also depicted and its features listed in Table 4.

Table 4. Summary of the major features for the INS spectra for ice-Ih measured at < 30K. [66, 67]

Energy (cm^{-1})	Putative Vibrational Mode
57	acoustic phonon region, translational mode
229	H bond (weak), translational mode
305	H bond (strong), translational mode
540	H bond librational band left edge
976	H bond librational band right edge

First, we start with some basic observations of Figure 6. There are 6 prominent features that increases in intensity with hydration at 90 cm^{-1}, 180 cm^{-1}, 520 cm^{-1}, 680, cm^{-1}, 770 cm^{-1} and 1000 cm^{-1}. Also notable is the broad feature ranging from 1300 – 2000 cm^{-1} that also slowly increases in intensity with hydration.

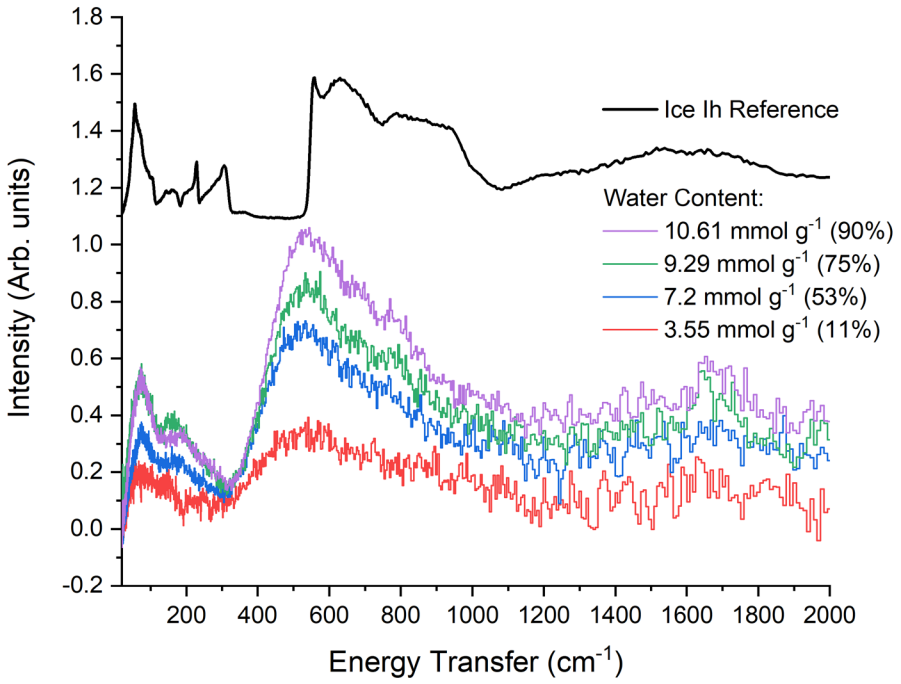

Figure 6. A water difference spectra and for comparison the spectra for ice. The hydrated melanin spectrum is subtracted from the dry spectrum subtracted to leave just the contribution from the added water. Legend indicates water content as well as corresponding relative humidity.

Given our discussion above about the computational cost that would be involved in modelling a representative melanin particle (a key requirement) alongside a water coating at different hydration levels, we are forced into having to interpret the water-melanin behaviour without the aid of theoretical calculations. As such, we will rely on qualitative knowledge of melanin and other model compounds for insight.

The best way to proceed is to compare and contrast the hydration dependent spectra against that of ice-Ih. We start with the most prominent feature of the data at 520 cm^{-1}, which for ice-Ih corresponds to the low energy edge of H-bond librations.[66, 67] As can be clearly seen, for ice-Ih the edge is sharp where as for the water in melanin it is significantly broadened. This behaviour is quite characteristic of amorphous forms of ice, both low density amorphous (LDA) ice and high density amorphous (HDA) ice.[66, 72-74] This immediately suggests that there is no long range crystal structure of ice-Ih present,

and as such if the sample was to be heated to room temperature, would imply no bulk water would be present in the polymer, even at high relative humidities. As such, the water within melanin is likely comprised entirely of this amorphous water or interfacial water. Indeed, we do not see a significant presence of bulk water due to the absence of any clear sharp edge to the libration low energy edge, which is commonly seen in other highly hydrated biopolymers.[68, 72, 73, 75] As an aside, this implies that the void structures that have been deduced within melanin structures elsewhere for water to fill,[38] are not conducive to bulk water formation.

From the observation of an acoustic vibrational modes seen in our data most prominently at 90 cm^{-1}, and to a lesser extent at 180 cm^{-1}, we can conclude that the water forms a continuous coating across the polymer and does not fill isolated pockets, even at low hydration content.[69]

Of interest is the absence of two translational, optical H-bond modes, which are present in ice-Ih at 229 cm^{-1} and 305 cm^{-1}. In ice-Ih these are due to two different H-bonds within ice, one weak and one strong, randomly distributed through a crystal structure.[66, 67] It is also known that the presence of these vibrations are not dependent on long range order but on local molecular conditions, since these peaks are also observed in LDA ice.[66] As such, the water in melanin spectra is much more akin to HDA ice, which do not have these two peaks.[66] Hence, we can deduce that the interfacial water within melanin is experiencing conditions such that standard hydrogen bond behaviour is not present, i.e. the water is highly confined. This naturally suggests that proton conducting mechanisms based upon standard bulk water is not applicable to melanin. This basic observation should bring into question the nature of the water structure and concomitant proton transport in other bioelectronic materials, which would need further investigation along the lines presented in this paper.

We now turn to comparing our results to other systems. Indeed, many of our broad features for the interfacial water behaviour have been observed in numerous bio/polymer water systems including DNA[72, 73, 75, 76] and proteolipid membranes[75], proteins[76], cell tissue[68], collagen and polypeptides[69]. In all these systems an absence of the translational hydrogen bonding modes are observed, and a large libration peak is seen with the concomitant straight-line decay from the peak (around 520 cm^{-1}) to around 1000 cm^{-1}. Our overall data set is slightly red shifted vs ice-Ih, in contrast to the observed blue shifts in the other works mentioned previously and to be expected by theoretical calculation where the latter was modelled on a polar groups of a surfactant molecule[77]. This red shift may simply be that the exact polar nature of the melanin particle surface is conducive to water libration modes that are lower in energy and may thus imply a strong connection to the melanin surface, as would be suggested by the large energy of adsorption seen in our BET isotherm data (Table 2).

Though, in line with theoretical work, as the hydration is increased, the relative intensity and blue shifting of the libration peak occurs as more hydration shells are added to water at the interface of the polar moieties on the hydrophilic surface[77]. As such, our data appears to be qualitatively as expected. Indeed, our lowest water content curve (~11% relative humidity) could be construed as the initial water layer locked to the surface of the melanin and its polar groups, which is also in line with the monolayer coverage point implied by the BET isotherm at ~ 0.1 relative pressure (10% relative humidity, see Figure 2 & Table 2). As the peaks increase in intensity a second, third and fourth layer of water is added. Considering that we do not observe bulk water formation, it does suggest that the number of layers of water does not extend far beyond 4 layers.

Given the nature of the water coating, it is logical to ask if one can get a firmer view on the number of water layers that are coating the melanin particles. The BET analysis performed on the adsorption isotherm of the powder melanin suggests ~ 5 layers of water (Figure 2, Table 2). This is more or less in line with the INS data and concomitant theoretical predictions just discussed. However, given the underlying assumptions of the BET theory (non-polar adsorbates), it would be prudent to perform a cross check against the literature. Our approach is to estimate the potential particle size of melanin and then determine the potential water coating around said particle. Regarding the particle sizes of synthetic melanin made as per our approach, multiple authors utilising different techniques have estimated sizes of ~1.5-2 nm [78-80], 2-3 nm[81], ~5 nm[82] and ~40 nm[83]. The latter result is an outlier and was deduced from light scattering experiments. The other studies are based upon more traditional morphological work including, X-ray, AFM, STM and TEM measurements and as such are more reliable. Furthermore, the more traditional studies have additional theoretical backing[84-86]. As such we have a range of average sizes to consider from ~1.5 – 5 nm. We select 5 nm as the example since this is confirmed by real space images from TEM measurements[82]. If one utilises the deduced density for an average melanin particle of 1.397 g cm^{-3} [78, 79], assume a spherical particle and a water density of 1.17 g cm^{-3} (in line with HDA ice at ambient conditions below 120 K[74]) at a relative humidity level of 90% (our highest level of hydration) one arrives at a water coverage of around 3 layers (see Supplementary Information). Considering that melanin particles will not be isolated but are compacted together, are not always spherical and have a distribution in different sizes, the number of layers appear to be more or less in line with the INS observations (~ 4 layers) as well as with the BET isotherm results (~ 5 layers). As such, we conclude that there is no bulk water formation in our sample. Furthermore, the INS data is confirmation of the BET analysis, which is quite surprising from a theoretical point of view.

We now turn to discrepancies with our observations and those of previous works. There are clear features present (at all hydration levels) at 650 – 700 cm^{-1}, 770 – 800 cm^{-1} and 900 – 1100 cm^{-1} that are entirely absent in all the other bio/water systems reported above and hence are unique to melanin. Instead, the closest results that we were able to find that correspond to these features can be found on hydrated zeolite systems[87, 88]. Interestingly, the speculation there is that these features could be due to the formation of charged species of water, e.g. hydronium.

Inspired by these observations, inspection of the literature of solid state proton conductors yields interesting interpretations. For example, the peaks could be assigned as Zundel ion ($H_5O_2^+$) modes for torsional (650 – 700 cm^{-1}), rock and wag (770 – 800 cm^{-1}) and an antisymmetric stretching hydrogen bonding vibration along an OHO bond (900 – 1100 cm^{-1}) [89-91]. A question to ask is where the symmetric counterpart is, which has been reported to be ~480 cm^{-1} [90, 91], which would be dominated by the water libration behaviour at around 550 cm^{-1} making it tenuous at best to assign.

At this juncture, one has two basic options, to assign these peaks to hydronium as suggest by the aforementioned zeolite studies or assigning the peaks to Zundel ion signatures. Currently, from the data as presented, it is not clear which given there is enough water layers to account for both species.

However, we can consider that the more stable ion in wet to aqueous environments is the Zundel ion[92, 93]. In addition, given that the zeolite works cited, which suggest hydronium, were performed at hydrations of up to 5% weight gain whereas our results go up to 18% weight gain[37], we tentatively suggest that the INS signatures we observe may be related to the Zundel ion.

One way to investigate the origin of these new features is to use another organic ionomer, which has a hydration dependent conductivity and that can be modelled with confidence. As such, Nafion[94] could be such a potential candidate, since its polymer structure is known and it has a hydration conductivity that exceeds that of melanin. Very recently, an INS/IR study of Nafion and a model compound triflouromethanesulfonic acid (CF_3SO_3H or TFSA) has been published[95], which can be used for comparison. A careful inspection of the INS – TOSCA data reveals that for low hydrated Nafion and associated TFSA, features similar to what is observed in Figure 6 at 650 – 700 cm^{-1} and 770 – 800 cm^{-1}. Indeed, the spectra in Figure 6 are similar to a potential amalgamation of 6.10 wt% hydrated Nafion (4.0 moles H_2O per SO_3) and 7.33 wt% hydrated Nafion (4.8 moles H_2O per SO_3), with some correspondence also to the Nafion soaked in water. The corresponding TFSA compounds would be hydrated with 2 or 4 water molecules, sufficient for the formation of the $H_5O_2^+$ cation, i.e. the Zundel ion. We note though that the authors indicated that $H_9O_4^+$ could also form at 4 molecules or more. Fascinatingly, the number of water molecules per acid group is similar to the number of water

layers for our system. Overall, it does appear that the features we observe and identify potentially as the Zundel ion in melanin may be a more general feature of soft, proton ionomer systems, provided that the number of water molecules available for solvation is kept to a level below that of bulk water formation.

Obviously, at this stage the $H_5O_2^+$ ion is a hypothetical particle in hydrated melanin and all signatures which we tried to attribute to it are indirect and based on correlation. To prove the existence of the Zundel ion will require more evidence. Given that melanin cannot be crystallized[31, 96, 97] and it is polyradical[47-49, 98], using the methods that have been used in other inorganic proton superionics will prove challenging. However, neutron scattering techniques will make crucial contributions into the studies of potential proton species dynamics and structure. Furthermore, precise examination of melanin for the $H_5O_2^+$ cation should also include Raman scattering study where the intensive band near 500 cm^{-1} should exist for the symmetric stretch. Probably, broad-band dielectric spectroscopy in the GHz-THz range should also assist, since the formation of $H_5O_2^+$ that has a relatively low dipole moment (compared to H_2O or H_3O^+) should decrease the general dielectric contribution $\Delta\varepsilon$ of water at these frequencies by well-known wide Debye relaxation [99]. Direct observation of unusual lowering or constant value of $\Delta\varepsilon$ for the main water Debye relaxation in course of melanin hydration would be a valuable evidence for $H_5O_2^+$ formation.

From the viewpoint of applications development, the $H_5O_2^+$ hypothesis suggests a need to shift traditional focus in methods of enhancement of melanin conductivity. Classical approach means doping of melanin with metal ions exchanging protons in carboxyl and semiquinone hydroxyl groups[100]. However, facilitated decomposition of $H_5O_2^+$ via thermal or chemical way may become a fruitful alternative in some cases.

Conclusions

In conclusion, we have performed a hydration dependent INS study on the biopolymer melanin. The method of hydration is new and rigorous to the INS family of techniques. We have investigated the dry spectra of melanin and modelled the spectra of this disorder oligomeric system as a superposition of the underlying monomer moieties of different oxidative states, yielding an acceptable result at low computational cost. We further investigated the hydration component of the spectra and conclude that the interfacial water in melanin is akin to high density amorphous ice. However, unlike previous hydrated biopolymer work, additional features have been observed, which we suggest are signatures of the Zundel ion. These features may be general for soft proton ionomer systems, if they are comprised of only interfacial water within their structure. The results open up new avenues for exploration in

elucidating the morphology of water and concomitant proton charge transport mechanism in bioelectronic materials.

Contributions

JAM-G & HC was responsible for the computational modelling of the dry spectra. ABM was responsible for sample synthesis, UV-Vis and EPR characterisation. JDMcG was responsible for XPS characterisation. ABM and HC was responsible for sample preparation and data acquisition on neutron beamline. HC was responsible for the data analysis. JAM-G, HC, KAM & ABM are responsible for the initial draft. All authors are responsible for the final draft. ABM, PM & KA are responsible for original conception of the project. ABM responsible for administrating the project.

Acknowledgements

J.A.M-G. acknowledge funding from the European Union's Horizon 2020 research and innovation programme under the Marie Skłodowska-Curie grant agreement No 665593 awarded to the Science and Technology Facilities Council. J.D.McG thank the EPSRC SPECIFIC project for funding (EP/N020863/1) & WEFO (ERDF) project AIM (80708 & EP/M015254/2) for their ongoing support for XPS maintenance. P.M. is a Sêr Cymru II National Research Chair, which is supported by the Welsh Government through the European Regional Development Fund and an Honorary Professor at the University of Queensland. K.A.M. acknowledge funding from Russian Science Foundation under grant 19-73-10154. A.B.M. is a Sêr Cymru II fellow and the results incorporated in this work is supported by the Welsh Government through the European Union's Horizon 2020 research and innovation program under the Marie Skłodowska-Curie grant agreement No 663830. A.B.M. thanks Mr. Iwan James, Mr. Jac Evans and Mr. Luke Jones for their help in obtaining the UV-Vis spectra. K.A.M. thanks Dr. Ivan Popov (Oak Ridge National Laboratory) for his important and enduring explanations related to collective water molecules dynamics and proton transfer mechanisms in solids. We thank the Electron Paramagnetic Group at Cardiff University and Dr. Emma Richards in particular for the use of their EPR equipment. We thank Dr. Svemir Rudic (ISIS Muon & Neutron Pulsed Facility) for help in collecting data. We also thank Dr. Stewart Parker at ISIS for the use of the ice-Ih spectra and Al spectra.

Conflict of Interest

There are no conflicts of interest to declare.

References

[1] M. Berggren, A. Richter-Dahlfors, Organic Bioelectronics, Advanced Materials 19 (2007) 3201-3213.
[2] P. Meredith, C.J. Bettinger, M. Irimia-Vladu, A.B. Mostert, P.E. Schwenn, Electronic and optoelectronic materials and devices inspired by nature, Reports on Progress in Physics 76 (2013) 034501.

[3] J. Rivnay, R.M. Owens, G.G. Malliaras, The Rise of Organic Bioelectronics, Chemistry of Materials 26 (2014) 679-685.
[4] P. Lin, F. Yan, Organic Thin-Film Transistors for Chemical and Biological Sensing, Advanced Materials 24 (2012) 34-51.
[5] A. Noy, Bionanoelectronics, Advanced Materials 23 (2011) 807-820.
[6] K. Svennersten, K.C. Larsson, M. Berggren, A. Richter-Dahlfors, Organic bioelectronics in nanomedicine, Biochimica Biophysica Acta - General Subjects 1810 (2011) 276-285.
[7] M. Muskovich, C.J. Bettinger, Biomaterials-Based Electronics: Polymers and Interfaces for Biology and Medicine, Advanced Healthcare Materials 1 (2012) 248-266.
[8] R.M. Owens, G.G. Malliaras, Organic Electronics at the Interface with Biology, MRS Bulletin 35 (2010) 449-456.
[9] G. Tarabella, F.M. Mohammadi, N. Copped, F. Barbero, S. Iannotta, C. Santato, F. Cicoira, New opportunities for organic electronics and bioelectronics: ions in action, Chemical Science 4 (2013) 1395-1409.
[10] N.A.o. Engineering, Grand Challenges for Engineering: Imperatives, Prospects, and Priorities., in: N.A.o. Engineering (Ed.), Grand Challenges for Engineering: Imperatives, Prospects, and Priorities., National Academies Press., Washington, 2016.
[11] N. Amdursky, E.D. Glowacki, P. Meredith, Macroscale Biomolecular Electronics and Ionics, Advanced Materials 31 (2019) 1802221.
[12] K. Tybrandt, R. Forchheimer, M. Berggren, Logic gates based on ion transistors, Nature Communications 3 (2012) 871.
[13] J. Rivnay, P. Leleux, M. Sessolo, D. Khodagholy, T. Herve, M. Fiocchi, G.G. Malliaras, Organic Electrochemical Transistors with Maximum Transconductance at Zero Gate Bias, Advanced Materials 25 (2013) 7010-7014.
[14] J. Rivnay, S. Inal, A. Salleo, R.M. Owens, M. Berggren, G.G. Malliaras, Organic Electrochemical Transistors, Nature Reviews Materials 3 (2018) 17086.
[15] C. Zhong, Y. Deng, A.F. Roudsari, A. Kapetanovic, M.P. Anantram, M. Rolandi, A polysaccharide bioprotonic field-effect transistor, Nature Communications 2 (2011) 476.
[16] Y. Deng, E. Josberger, J. Jin, A.F. Roudsari, B.H. Helms, C. Zhong, M.P. Anantram, M. Rolandi, H+ -type and OH- -type biological protonic semiconductors and complementary devices, Scientific Reports 3 (2013) 2481.
[17] A.B. Mostert, B.J. Powell, F.L. Pratt, G.R. Hanson, T. Sarna, I.R. Gentle, P. Meredith, Role of semiconductivity and ion transport in the electrical conduction of melanin, Proceedings of the National Academy of Sciences USA 109 (2012) 8943-8947.
[18] J. Wünsche, Y. Deng, P. Kumar, E. Di Mauro, E. Josberger, J. Sayago, A. Pezzella, F. Soavi, F. Cicoira, M. Rolandi, C. Santanto, Protonic and Electronic Transport in Hydrated Thin Films of the Pigment Eumelanin, Chemistry of Materials 27 (2015) 436-442.
[19] M. Sheliakina, A.B. Mostert, P. Meredith, Decoupling Ionic and Electronic Currents in Melanin, Advanced Functional Materials 28 (2018) 1805514.
[20] D.D. Ordinario, L. Phan, W.G. Walkup IV, J.-M. Jocson, E. Karshalev, N. Husken, A.A. Gorodetsky, Bulk protonic conductivity in a cephalopod structural protein, Nature Chemistry 6 (2014) 596-602.
[21] D.D. Ordinario, L. Phan, J.-M. Jocson, T. Nguyen, A.A. Gorodetsky, Protonic transistors from thin reflectin films, APL Materials 3 (2015) 014907.
[22] E.E. Josberger, P. Hassanzadeh, Y. Deng, J. Sohn, M.J. Rego, C.T. Amemiya, M. Rolandi, Proton conductivity in ampullae of Lorenzini jelly, Science Advances 2 (2016) e1600112.
[23] J. Selberg, M. Jia, M. Rolandi, Proton conductivity of glycosaminoglycans, PLoS ONE 14 (2019) e0202713.
[24] D. Mawad, C. Mansfield, A. Lauto, F. Perbellini, G.W. Nelson, J. Tonkin, S.O. Bello, D.J. Carrad, A.P. Micolich, M.M. Mahat, J. Furman, D.J. Payne, A.R. Lyon, J.J. Gooding, S.E. Harding, C.M. Terracciano, M.M. Stevens, A conducting polymer with enhanced electronic stability applied in cardiac models, Science Advances 2 (2016) e1601007.

[25] N. Amdursky, X. Wang, P. Meredith, D.D.C. Bradley, M.M. Stevens, Long-Range Proton Conduction across Free-Standing Serum Albumin Mats, Advanced Materials 28 (2016) 2692-2698.
[26] D.J. Carrad, A.B. Mostert, A.R. Ullah, A.M. Burke, H.J. Joyce, H.H. Tan, C. Jagadish, P. Krogstrup, J. Nygard, P. Meredith, A.P. Micolich, Hybrid nanowire ion-to-electron transducers for integrated bioelectronic circuitry, Nano Letters 17 (2017) 827-833.
[27] J.G. Gluschke, J. Seidl, R.W. Lyttleton, K. Nguyen, M. Lagier, F. Meyer, P. Krogstrup, J. Nygård, S. Lehmann, A.B. Mostert, P. Meredith, A.P. Micolich, Integrated bioelectronic proton-gated logic elements utilizing nanoscale patterned Nafion, Materials Horizons 8 (2021) 224-233.
[28] D. Nilsson, T. Kugler, P.-O. Svensson, M. Berggren, An all-organic sensor–transistor based on a novel electrochemical transducer concept printed electrochemical sensors on paper, Sensors and Actuators B: Chemical 86(2) (2002) 193-197.
[29] Y. van de Burgt, E. Lubberman, E.J. Fuller, S.T. Keene, G.C. Faria, S. Agarwal, M.J. Marinella, A.A. Talin, A. Salleo, A non-volatile organic electrochemical device as a low-voltage artificial synapse for neuromorphic computing, Nature Materials 16 (2017) 414-419.
[30] Y. Agam, R. Nandi, T. Bulava, N. Amdursky, The role of the protein–water interface in dictating proton conduction across protein-based biopolymers, Materials Advances 2(5) (2021) 1739-1746.
[31] P. Meredith, T. Sarna, The physical and chemical properties of eumelanin, Pigment Cell Research 19 (2006) 572-594.
[32] M. Sheliakina, A.B. Mostert, P. Meredith, An All-Solid-State Biocompatible Ion-to-Electron Transducer for Bioelectronics, Material Horizons 5 (2018) 256-263.
[33] M. Ambrico, P.F. Ambrico, A. Cardone, T. Ligonzo, S.R. Cicco, R. Di Mundo, V. Augelli, G.M. Farinola, Melanin Layer on Silicon: an Attractive Structure for a Possible Exploitation in Bio-Polymer Based Metal-Insulator-Silicon Devices, Advanced Materials 23 (2011) 3332.
[34] P. Kumar, E. Di Mauro, S. Zhang, A. Pezzella, F. Soavi, C. Santato, F. Cicoira, Melanin-based flexible supercapacitors, Journal of Materials Chemistry C 4 (2016) 9516-9525.
[35] Y.J. Kim, W. Wu, S. Chun, J.F. Whitacre, C.J. Bettinger, Biologically derived melanin electrodes in aqueous sodium-ion energy storage devices, Proceedings of the National Academy of Sciences USA 110 (2013) 20912-20917.
[36] Z. Tehrani, S.P. Whelan, B. Mostert, J.V. Paulin, M.M. Ali, E.D. Ahmadi, C.F.O. Graeff, O.J. Guy, D.T. Gethin, Printable and Flexible Graphene pH sensors utilising Thin Film Melanin for Physiological Applications, 2D Materials 7 (2020) 024008.
[37] A.B. Mostert, K.J.P. Davy, J.L. Ruggles, B.J. Powell, I.R. Gentle, P. Meredith, Gaseous adsorption in melanins: Hydrophilic biomacromolecules with high electrical conductivities, Langmuir 26 (2010) 412-416.
[38] A.J. Clulow, A.B. Mostert, M. Sheliakina, A. Nelson, N. Booth, P.L. Burn, I.R. Gentle, P. Meredith, The structural impact of water sorption on device-quality melanin thin films, Soft Matter 13 (2017) 3954-3965.
[39] K.A. Motovilov, V. Grinenko, M. Savinov, Z.V. Gagkaeva, L.S. Kadyrov, A.A. Pronin, Z.V. Bedran, E.S. Zhukova, A.B. Mostert, B.P. Gorshunov, Redox chemistry in the pigment eumelanin as a function of temperature using broadband dielectric spectroscopy, RSC Advances 9 (2019) 3857-3867.
[40] M. Reali, A. Gouda, J. Bellemare, D. Ménard, J.-M. Nunzi, F. Soavi, C. Santato, Electronic Transport in the Biopigment Sepia Melanin, ACS Applied Bio Materials 3(8) (2020) 5244-5252.
[41] P. Mitchell, S. Parker, A. Ramirez-Cuesta, J. Tomkinson, Vibrational Spectroscopy with Neutrons - With Applications In Chemistry, Biology, Materials Science And Catalysis, World Scientific Publishing Co Pte Ltd2005.
[42] S.F. Parker, D. Lennon, P.W. Albers, Vibrational Spectroscopy with Neutrons: A Review of New Directions, Applied Spectroscopy 65(12) (2011) 1325–1341.
[43] H. Cavaye, Neutron Spectroscopy: An Under-Utilised Tool for Organic Electronics Research?, Angewandte Chemie International Edition 58(28) (2019) 1433-7851.
[44] C.C. Felix, J.S. Hyde, T. Sarna, R.C. Sealy, Interactions of melanin with metal ions. Electron spin resonance evidence for chelate complexes of metal ions with free radicals., Journal of the American Chemical Society 100 (1978) 3922-3926.

[45] M. d'Ischia, K. Wakamatsu, A. Napolitano, S. Briganti, J.C. Garcia-Borron, D. Kovacs, P. Meredith, A. Pezzella, M. Picardo, T. Sarna, J.D. Simon, S. Ito, Melanins and melanogenesis: methods, standards, protocols, Pigment Cell Research 26 (2013) 616-633.
[46] P. Meredith, B.J. Powell, J. Riesz, S.P. Nighswander-Rempel, M.R. Pederson, E.G. Moore, Towards structure–property–function relationships for eumelanin, Soft Matter 2 (2006) 37-44.
[47] A.B. Mostert, G.R. Hanson, T. Sarna, I.R. Gentle, B.J. Powell, P. Meredith, Hydration-Controlled X-Band EPR Spectroscopy: A Tool for Unravelling the Complexities of the Solid-State Free Radical in Eumelanin, Journal of Physical Chemistry B 117 (2013) 4965-4972.
[48] J.V. Paulin, A. Batagin-Neto, P. Meredith, C.F.O. Graeff, A.B. Mostert, Shedding Light on the Free Radical Nature of Sulfonated Melanins, The Journal of Physical Chemistry B 124(46) (2020) 10365-10373.
[49] A.B. Mostert, S.B. Rienecker, C. Noble, G.R. Hanson, P. Meredith, The photoreactive free radical in eumelanin, Science Advances 4 (2018) eaaq1293.
[50] J.V. Paulin, J.D. McGettrick, C.F.O. Graeff, A.B. Mostert, Melanin system composition analyzed by XPS depth profiling, Surfaces and Interfaces 24 (2021) 101053.
[51] S.B. Rienecker, A.B. Mostert, G. Schenk, G.R. Hanson, P. Meredith, Heavy water as a probe of the free radical nature and electrical conductivity of melanin, Journal of Physical Chemistry B 119 (2015) 14994-15000.
[52] G. Barnes, I. Gentle, Interfacial Science: An Introduction, 2nd ed., Oxford University Press2011.
[53] B. Mostert, J. Paulin, B. Gorshunov, H. Cavaye, K. Motovilov, P. Meredith, J. Martinez-Gonzalez, Melanin's vibrational behaviour as a function of temperature and hydration to give insight to its heat capacity and conductivity behaviour, in: S.I.N.a.M. Source (Ed.) 2019.
[54] D. Colognesi, M. Celli, F. Cilloco, R.J. Newport, S.F. Parker, V. Rossi-Albertini, F. Sacchetti, J. Tomkinson, M. Zoppi, TOSCA neutron spectrometer: The final configuration, Applied Physics A: Materials Science & Processing 74 (2002) S64-S66.
[55] S.F. Parker, F. Fernandez-Alonso, A.J. Ramirez-Cuesta, J. Tomkinson, S. Rudic, R.S. Pinna, G. Gorini, J. Fernández Castañon, Recent and future developments on TOSCA at ISIS, Journal of Physics: Conference Series 554 (2014) 012003.
[56] I.N.a.M. Source, 2020.
[57] O. Arnold, J.C. J.C. Bilheux, J.M. Borreguero, A. Buts, S.I. Campbell, L. Chapon, M. Doucet, N. Draper, R. Ferraz Leal, M.A. Gigg, V.E. Lynch, A. Markvardsen, D.J. Mikkelson, R.L. Mikkelson, R. Miller, K. Palmen, P. Parker, G. Passos, T.G. Perring, P.F. Peterson, S. Ren, M.A. Reuter, A.T. Savici, J.W. Taylor, R.J. Taylor, R. Tolchenov, W. Zhou, J. Zikovsky, Mantid—Data analysis and visualization package for neutron scattering and μSR experiments, Nuclear Instruments and Methods in Physics Research A 764 (2014) 156-166.
[58] V.F. Sears, Neutron scattering lengths and cross sections, Neutron News 3(3) (1992) 26-37.
[59] J. Tomkinson, J. Riesz, P. Meredith, S.F. Parker, The vibrational spectrum of indole: An inelastic neutron scattering study, Chemical Physics 345(2) (2008) 230-238.
[60] M.J. Frisch, G.W. Trucks, H.B. Schlegel, G.E. Scuseria, M.A. Robb, J.R. Cheeseman, G. Scalmani, V. Barone, G.A. Petersson, H. Nakatsuji, X. Li, M. Caricato, A.V. Marenich, J. Bloino, B.G. Janesko, R. Gomperts, B. Mennucci, H.P. Hratchian, J.V. Ortiz, A.F. Izmaylov, J.L. Sonnenberg, D. Williams-Young, F. Ding, F. Lipparini, F. Egidi, J. Goings, B. Peng, A. Petrone, T. Henderson, D. Ranasinghe, V.G. Zakrzewski, J. Gao, N. Rega, G. Zheng, W. Liang, M. Hada, M. Ehara, K. Toyota, R. Fukuda, J. Hasegawa, M. Ishida, T. Nakajima, Y. Honda, O. Kitao, H. Nakai, T. Vreven, K. Throssell, J.A. Montgomery Jr., J.E. Peralta, F. Ogliaro, M.J. Bearpark, J.J. Heyd, E.N. Brothers, K.N. Kudin, V.N. Staroverov, T.A. Keith, R. Kobayashi, J. Normand, K. Raghavachari, A.P. Rendell, J.C. Burant, S.S. Iyengar, J. Tomasi, M. Cossi, J.M. Millam, M. Klene, C. Adamo, R. Cammi, J.W. Ochterski, R.L. Martin, K. Morokuma, O. Farkas, J.B. Foresman, D.J. Fox, Gaussian 16, Gaussian, Inc., Wallingford, CT, 2016.
[61] A.D. Becke, Density-functional thermochemistry. III. The role of exact exchange, Journal of Chemical Physics 98 (1993) 5648-5652.
[62] C. Lee, W. Yang, R.G. Parr, Development of the Colle-Salvetti correlation-energy formula into a functional of the electron density, Physical Review B 37 (1988) 785-789

[63] K. Dymkowski, S.F. Parker, F. Fernandez-Alonso, S. Mukhopadhyay, AbINS: The modern software for INS interpretation, Physica B: Condensed Matter 551 (2018) 443-448.
[64] S. Ito, A chemist's view of melanogenesis, Pigment Cell Research 16 (2003) 230-236.
[65] A.B. Mostert, On the free radical redox chemistry of 5,6-dihydroxyindole, Chemical Physics 546 (2021) 111158.
[66] J. Li, Inelastic neutron scattering studies of hydrogen bonding in ices, The Journal of Chemical Physics 105(16) (1996) 6733-6755.
[67] J. Li, D.K. Ross, Evidence for two kinds of hydrogen bond in ice, Nature 365(6444) (1993) 327-329.
[68] R.C. Ford, S.V. Ruffle, A.J. Ramirez-Cuesta, I. Michalarias, I. Beta, A. Miller, J. Li, Inelastic Incoherent Neutron Scattering Measurements of Intact Cells and Tissues and Detection of Interfacial Water, Journal of the American Chemical Society 126(14) (2004) 4682-4688.
[69] H.D. Middendorf, R.L. Hayward, S.F. Parker, J. Bradshaw, A. Miller, Vibrational neutron spectroscopy of collagen and model polypeptides, Biophysical Journal 69(2) (1995) 660-673.
[70] P.J. Gonçalves, O.B. Filho, C.F.O. Graeff, Effects of hydrogen on the electronic properties of synthetic melanin, Journal of Applied Physics 99 (2006) 104701.
[71] C.T. Chen, F.J. Martin-Martinez, G.S. Jung, M.J. Buehler, Polydopamine and eumelanin molecular structures investigating with ab initio calculations, Chemical Science 8 (2017) 1631-1641.
[72] I. Michalarias, I. Beta, R. Ford, S. Ruffle, J.C. Li, Inelastic neutron scattering studies of water in DNA, Applied Physics A 74(1) (2002) s1242-s1244.
[73] I. Michalarias, I.A. Beta, J.C. Li, S. Ruffle, R. Ford, The interaction of water with DNA — a combined inelastic neutron scattering and infrared spectroscopic study, Journal of Molecular Liquids 101(1) (2002) 19-26.
[74] A.I. Kolesnikov, J. Li, S.F. Parker, R.S. Eccleston, C.K. Loong, Vibrational dynamics of amorphous ice, Physical Review B 59(5) (1999) 3569-3578.
[75] S.V. Ruffle, I. Michalarias, J.-C. Li, R.C. Ford, Inelastic Incoherent Neutron Scattering Studies of Water Interacting with Biological Macromolecules, Journal of the American Chemical Society 124(4) (2002) 565-569.
[76] I. Michalarias, X. Gao, R.C. Ford, J. Li, Recent progress on our understanding of water around biomolecules, Journal of Molecular Liquids 117(1) (2005) 107-116.
[77] S. Pal, S. Balasubramanian, B. Bagchi, Dynamics of bound and free water in an aqueous micellar solution: Analysis of the lifetime and vibrational frequencies of hydrogen bonds at a complex interface, Physical Review E 67(6) (2003) 061502.
[78] J.I.N. Cheng, S.C. Moss, M. Eisner, P. Zschack, X-Ray Characterization of Melanins—I, Pigment Cell Research 7(4) (1994) 255-262.
[79] J.I.N. Cheng, S.C. Moss, M. Eisner, X-Ray Characterization of Melanins—II, Pigment Cell Research 7(4) (1994) 263-273.
[80] G.W. Zajac, J.M. Gallas, J. Cheng, M. Eisner, S.C. Moss, A.E. Alvarado-Swaisgood, The fundamental unit of synthetic melanin: a verification by tunneling microscopy of x-ray scattering results, Biochimica et Biophysica Acta 1199 (1994) 271-278.
[81] G.S. Lorite, V.R. Coluci, M.I.N. da Silva, S.N. Dezidério, C.F.O. Graeff, D.S. Galvão, M.A. Cotta, Synthetic melanin films: Assembling mechanisms, scaling behavior, and structural properties, Journal of Applied Physics 99(11) (2006) 113511.
[82] A.A.R. Watt, J.P. Bothma, P. Meredith, The Supramolecular Structure of Melanin., Soft Matter 5 (2009) 3754-3760.
[83] J. Riesz, J. Gilmore, P. Meredith, Quantitative Scattering of Melanin Solutions, Biophysical Journal 90 (2006) 4137–4144.
[84] K.B. Stark, J.M. Gallas, G.W. Zajac, M. Eisner, J.T. Golab, Spectroscopic study and simulation from recent structural models for eumelanin: II: oligomers, Journal of Physical Chemistry B 107 (2003) 11558-11562.
[85] K.B. Stark, J.M. Gallas, G.W. Zajac, M. Eisner, J.T. Golab, Spectroscopic Study and Simulation from Recent Structural Models for Eumelanin: I. Monomer, Dimers, The Journal of Physical Chemistry B 107(13) (2003) 3061-3067.

[86] K.B. Stark, J.M. Gallas, G.W. Zajac, J.T. Golab, S. Gidanian, T. McIntire, P.J. Farmer, Effect of Stacking and Redox State on Optical Absorption Spectra of Melanins-Comparison of Theoretical and Experimental Results, Journal of Physical Chemistry B 109 (2005) 1970-1977.
[87] C. Corsaro, V. Crupi, D. Majolino, S.F. Parker, V. Venuti, U. Wanderlingh, Inelastic Neutron Scattering Study of Water in Hydrated LTA-Type Zeolites, The Journal of Physical Chemistry A 110(3) (2006) 1190-1195.
[88] M. Jiménez-Ruiz, D.S. Gahle, T. Lemishko, S. Valencia, G. Sastre, F. Rey, Evidence of Hydronium Formation in Water–Chabazite Zeolite Using Inelastic Neutron Scattering Experiments and ab Initio Molecular Dynamics Simulations, The Journal of Physical Chemistry C 124(9) (2020) 5436-5443.
[89] D.J. Jones, J. Rozière, Complementarity of optical and incoherent inelastic neutron scattering spectroscopies in the study of proton conducting materials, Solid State Ionics 61(1) (1993) 13-22.
[90] D.J. Jones, J. Rozière, J. Penfold, J. Tomkinson, Incoherent inelastic neutron scattering studies of proton conducting materials trivalent metal acid sulphate hydrates: Part I. The vibrational spectrum of H5O2+, Journal of Molecular Structure 195 (1989) 283-291.
[91] U.B. Mioc, P. Colomban, M. Davidovic, J. Tomkinson, Inelastic neutron scattering study of protonic species during the thermal dehydration of 12-tungstophosphoric hexahydrate, Journal of Molecular Structure 326 (1994) 99-107.
[92] M.V. Vener, N.B. Librovich, The structure and vibrational spectra of proton hydrates: as a simplest stable ion, International Reviews in Physical Chemistry 28(3) (2009) 407-434.
[93] M. Thämer, L. De Marco, K. Ramasesha, A. Mandal, A. Tokmakoff, Ultrafast 2D IR spectroscopy of the excess proton in liquid water, Science 350(6256) (2015) 78.
[94] K.A. Mauritz, R.B. Moore, State of Understanding Nafion, Chemical Reviews 104 (2004) 4535-4585.
[95] S.F. Parker, S. Shah, Characterisation of hydration water in Nafion membrane, RSC Advances 11(16) (2021) 9381-9385.
[96] M. d'Ischia, A. Napolitano, A. Pezzella, P. Meredith, M. Buehler, Melanin Biopolymers: Tailoring Chemical Complexity for Materials Design, Angewandte Chemie International Edition 59(28) (2020) 11196-11205.
[97] M. d'Ischia, K. Wakamatsu, F. Cicoira, E.D. Mauro, J.C. Garcia-Borron, S. Commo, I. Galvan, G. Ghanem, K. Kenzo, P. Meredith, A. Pezzella, C. Santanto, T. Sarna, J.D. Simon, L. Zecca, F.A. Zucca, A. Napolitano, S. Ito, Melanins and melanogenesis: from pigment cells to human health and technological applications, Pigment Cell Melanoma Research 28 (2015) 520-544.
[98] A. Batagin-Neto, E.S. Bronze-Uhle, C.F.O. Graeff, Electronic structure calculations of ESR parameters of melanin units, Phys. Chem. Chem. Phys. 17 (2015) 7264-7274.
[99] I. Popov, P.B. Ishai, A. Khamzin, Y. Feldman, The mechanism of the dielectric relaxation in water, Physical Chemistry Chemical Physics 18(20) (2016) 13941-13953.
[100] A.B. Mostert, S. Rienecker, M. Sheliakina, P. Zierep, G.R. Hanson, J.R. Harmer, G. Schenk, P. Meredith, Engineering Proton Conductivity in Melanin Using Metal Doping, Journal of Materials Chemistry B (2020).